Available online at www.sciencedirect.com
SCIENCE DIRECT®
International Journal of Heat and Mass Transfer 49 (2006) 962–974
International Journal of HEAT and MASS TRANSFER
www.elsevier.com/locate/ijhmt

Evaporative heat transfer characteristics of a water spray on micro-structured silicon surfaces

Cheng-Chieh Hsieh, Shi-Chune Yao *

Department of Mechanical Engineering, Carnegie Mellon University, 5000 Forbes Avenue, Pittsburgh, PA 15213, USA

Received 26 October 2004; received in revised form 14 September 2005
Available online 21 November 2005

Abstract

Experiments were performed to evaluate the evaporative heat transfer characteristics of spray cooling of water on plain and micro-structured silicon surfaces at very low spray mass fluxes. The textured surface is made of an array of square micro-studs. It was found that the Bond number of the microstructures is the primary factor responsible for the heat transfer enhancement of evaporative spray cooling on micro-structured silicon surface in the present study. A qualitative study of evaporation of a single water droplet on plain and textured silicon surface shows that the capillary force within the microstructures is effective in spreading the deposited liquid film, thus increasing the evaporation rates. Four distinct heat transfer regimes, which are the flooded, thin film, partial dryout, and dryout regimes, were identified for evaporative spray cooling on micro-structured silicon surfaces. The microstructures provided better cooling performance in the thin film and partial dryout regime and higher liquid film breakup heat flux, because more water was retained on the heat transfer surface due to the capillary force. Heat transfer coefficient and temperature stability deteriorated greatly once the liquid film breakup occurred. The liquid film breakup heat flux increases with the Bond number. Effects of surface material, system orientation and spray mass flux were also addressed in this study.

Keywords: Evaporative heat transfer; Spray cooling; Capillary force; Surface enhancement; Silicon

1. Introduction

Despite the intense efforts in reducing the heat generation by integrated circuits, the continuous pursuit of faster clock speeds and higher packaging density of microprocessors has substantiated the need for more effective thermal management schemes than the conventional air cooling techniques to assure reliable electronics operation. Liquid cooling for high-heat-flux electronics thermal management has been extensively investigated in the past two decades. To provide maximum cooling efficiency, the liquid coolant is always allowed to undergo the liquid–vapor phase change process. Moreover, unlike the single-phase cooling, in which the surface temperature varies linearly with the heat flux, the phase-change heat transfer allows small temperature changes for large variations of the imposed heat flux because of the utilization of the latent heat of vaporization.

Compared to other phase-change cooling techniques for high-heat-flux electronics, such as direct liquid immersion cooling [1,2], microchannel cooling [3,4] and jet impingement cooling [5,6], spray cooling appears more promising for electronics cooling applications. Spray cooling with phase-change has been demonstrated to be an effective means to remove huge amount of heat with a low surface superheat [6–9]. The nature of dispersed droplet impingement in a spray cooling system gives rise to a more uniform spatial surface temperature distribution over the entire spray impact area. Boiling incipient superheat, which may cause a severe thermal shock to electronic components and make the heat transfer performance highly unpredictable, is much less pronounced in spray cooling systems than in pool or flow boiling systems [6,7]. This can be

* Corresponding author. Tel.: +1 412 268 2508; fax: +1 412 268 3348.
E-mail address: scyao@cmu.edu (S.-C. Yao).

0017-9310/$ - see front matter © 2005 Elsevier Ltd. All rights reserved.
doi:10.1016/j.ijheatmasstransfer.2005.09.013

Nomenclature

G	groove width (m)
g	gravitational constant (N/s^2)
h	heat transfer coefficient (W/m^2 K)
T	temperature (k)
Greek symbols	
γ	surface tension (N/m)
ρ	density (kg/m^3)
Superscript	
S	extrapolated surface temperature
Subscripts	
1, 2	temperature measuring point
l	liquid phase
v	vapor phase

attributed to the fact that the deposited liquid film is so thin that the bubble nucleation from the surface is significantly suppressed, allowing the spray-entrained gas embryos to serve as preferred nucleate sites such that surface nucleation is impeded [7]. Spray cooling can also provide significantly higher critical heat fluxes (CHF), the upper thermal design limit for any phase-change cooling system, than jet impingement cooling for given flow rates [6]. CHF values in spray cooling are found to be limited mainly by the liquid supply [10] and insensitive to heat flux fluctuations [6], making spray cooling a safer approach for electronic cooling than jet cooling.

A variety of surface modification techniques have been successfully developed to improve the heat transfer performance of spray cooling. Pais et al. [11] used air-atomized nozzles to spray very fine water droplets (7–28 μm) on different copper surfaces having roughness ranging from 0.1 to 1.2 μm, and concluded that smooth surfaces have higher heat transfer due to the thinner liquid film formed on surfaces. However, Sehmbey et al. [9] showed the opposite results in their liquid nitrogen spray cooling with copper surfaces having roughness ranging from 0.05 to 0.15 μm. They attributed the contradiction to the different wettability of water and liquid nitrogen with copper surface. Spray cooling on coated microporous surfaces has been investigated experimentally by Kim et al. [12] recently. They found that the coated surfaces perform better than a plain surface, because the microporous coating is able to delay the occurrence of surface dryout.

Evaporation by conduction through the thin liquid film formed by the impacting droplets can be the dominant heat transfer mechanism in a spray cooling system [10,13]. The relative contribution of this thin film evaporation increases as the spray mass flux decreases [14]. Therefore, the establishment of a thinner liquid film on the whole heat transfer surface is very desirable in an evaporative spray cooling system.

In the present study, evaporative spray cooling of water on silicon surfaces at extremely low spray mass fluxes was encountered. Since silicon is not a good wettable material for water, the silicon chips were modified by creating microstructures on the surface to achieve maximum cooling performance. The capillary force within the microstructures is believed to not only retain more water for heat dissipation, but also induce more effective liquid spreading for thinner liquid film to improve the evaporative heat transfer and surface temperature uniformity. The primary objective of the current study is to develop a general understanding of the evaporative heat transfer characteristics of spray cooling of water on micro-textured silicon surfaces at very low spray mass fluxes. Different surface textures were tested to reveal the effects of surface texture. Furthermore, experiments of different surface materials, spray mass fluxes and system orientations were carried out to examine their effects on evaporative spray cooling performance.

2. Experimental details

2.1. Micro-textured silicon surface

The surface enhancement is realized by an array of square studs. The microstructures on the heating surface not only increase the heat transfer area but also provide a driving force for liquid spreading. To characterize the capillary force between micro-studs, a dimensionless parameter, Bond number (Bo), is adopted.

$$Bo = \frac{G}{\sqrt{\gamma/(\rho_l - \rho_v)g}} \tag{1}$$

The Bond number is a comparison between gravitational force and the surface tension force. Generally, narrower grooves (smaller Bo's) are more desirable in evaporative heat transfer because of the better liquid spreading ability. Nevertheless, down to a critical Bond number where the grooves will be too small to allow the deposited liquid film to penetrate and flow freely (at the limiting case it appears similar to a flat smooth surface), the benefits of stronger capillary force begin to diminish. Hence, there may exist an optimal groove width for the evaporative water spray cooling on enhanced silicon surfaces. Another influential surface factor in current study is the bottom surface area of the grooves, because it is directly related to the surface area available for the liquid evaporation in the grooves.

Three surface textures were investigated and their geometric parameters are listed in Table 1. The test surfaces are specified by their groove width and stud size;

Table 1
Geometric parameters of the tested surfaces

Surface code	Plain Si	120G × 160S	120G × 480S	360G × 480S	Plain Al
Material	Silicon	Silicon	Silicon	Silicon	Aluminum
Roughness (μm)	0.003	–	–	–	0.338
Groove width (μm)	–	120	120	360	–
Stud size (μm)	–	160	480	480	–
Groove depth (μm)	–	333.3	335.2	454.8	–
Bond no. @ 25 °C	–	0.044	0.044	0.130	–
A_G/A_B area ratio[a]	–	0.67	0.36	0.67	–
Area augmentation	0	2.72	1.79	1.24	0

[a] A_G is the total bottom surface area of the grooves, and A_B is the base area, $25.2 \times 25.2\ mm^2$.

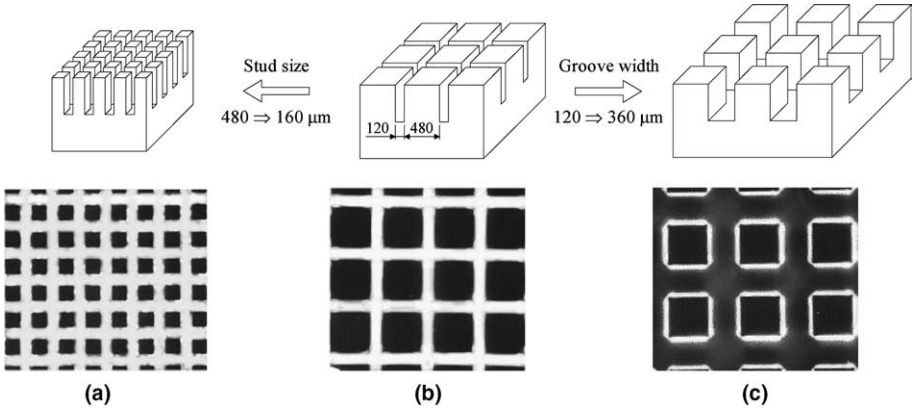

Fig. 1. Schematics and microphotographs of the three micro-structured silicon surfaces fabricated by DRIE.

that is, 120G × 160S (Fig. 1(a)), 120G × 480S (Fig. 1(b)) and 360G × 480S (Fig. 1(c)). Surfaces 120G × 160S and 120G × 480S have the same Bond number but different groove bottom surface area; on the other hand, surface 120G × 160S and 3600G × 480S only differ in Bond number. An inductively coupled plasma (ICP) deep reactive ion etching (DRIE) system (Surface Technology Systems) was used to fabricate the micro-studs on a 1000-μm thick, single-side polished (1 0 0) silicon wafer. The DRIE allows anisotropic etching and can create high-aspect-ratio microstructures with nearly vertical walls and straight-cut openings. The depth of the etched grooves on different textured silicon surfaces was measured to be between 333 and 455 μm using an optical microscope with a resolution of 0.1 μm along the *Z*-axis. After DRIE, the wafer was placed into an O_2 plasma etcher for 20 min to remove photoresist residues as well as to oxidize the surface. The wafer was then cut into a $46.4 \times 46.4\text{-mm}^2$ die with a micro-textured area of $25.2 \times 25.2\ mm^2$ at the center.

A plain test chip without any surface modification was used as reference for heat transfer performance comparison. In addition, a polished aluminum (alloy 6061-T6) plate was used to reveal the effect of surface material on evaporative spray cooling of water. The aluminum test chip was finished with emery sandpapers at increasing grits of 320, 400 and 600. The surface profiles of the plain silicon and aluminum surfaces were measured along a 300-μm line by an optical profilometer (Wyko NT3300, Veeco). The plain silicon surface has a geometric average roughness of 0.003 μm with a standard deviation of 0.003 μm, and the aluminum surface 0.338 and 0.245 μm. The maximum protrusion/indention within the assessment length is 0.014 and 1.531 μm for the plain silicon and aluminum surface, respectively.

2.2. Experimental setup

The experimental apparatus is schematically depicted in Fig. 2. Two different setups were used in this study to investigate the evaporative heat transfer characteristics at low and high spray mass flux. The two systems differ in three aspects: type of heater, liquid supply method, and spray nozzle capacity. The open test system is divided into three major subsystems: fluid supply and spray system, miniaturized test bed, and data acquisition system.

2.2.1. Fluid supply and spray system

As shown in Fig. 2, the fluid supply and spray system consists of a rotary vacuum pump, a stainless steel water tank, two in-line pressure regulators, a pressure gauge and a spray nozzle. For low spray mass flux tests, the liquid was driven by a metering diaphragm pump, while pre-purified compressed nitrogen gas was used to pressurize the water tank for liquid supply in high-heat-flux tests. A

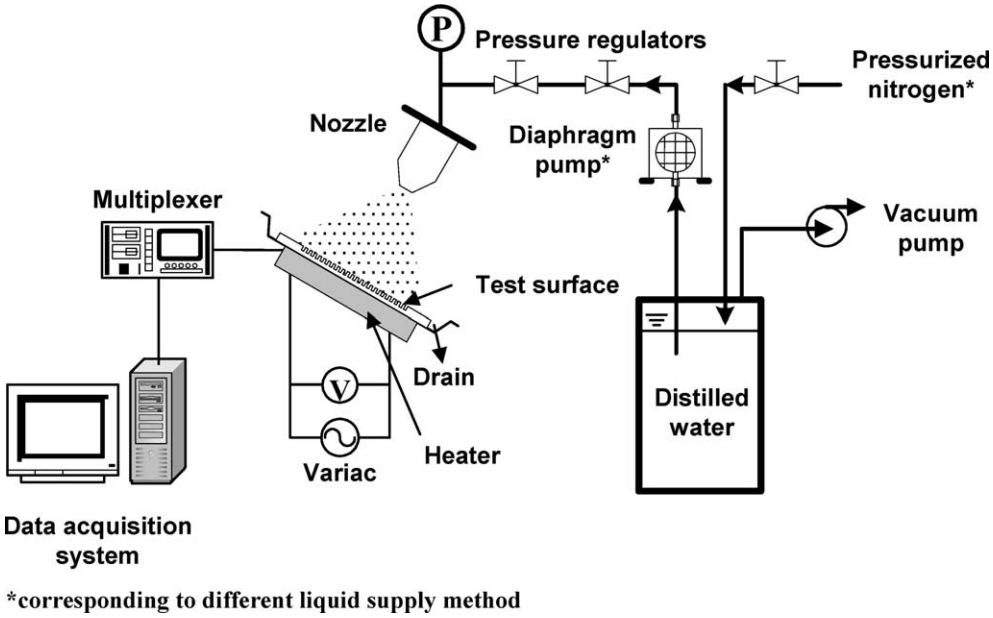

Fig. 2. Experimental setup of the evaporative spray cooling system.

strainer was installed just right before the nozzle to filter out particles of micron size. To maintain constant water quality throughout all tests, double distilled water was used. Water was selected as the working fluid because of its availability and superior thermal transport properties as compared to refrigerants.

For the low spray mass flux tests, a spray nozzle (WDB-0.5, Delevan) with a spray angle of 80° and an orifice diameter of 0.21 mm, was used. A nozzle (WDB-2.0, Delevan) with a spray angle of 60° and an orifice diameter of 0.38 mm was used for the high spray mass flux tests. Both spray nozzles are pressurized full-cone nozzles. The droplet distribution across the cross-section of the sprays is fairly uniform with a slight depression in the center of the spray. As specified by the manufacturer, the WDB-0.5 and WDB-2.0 nozzles produce water droplets of about 75 and 100 μm Sauter mean diameter (d_{32}), respectively, at 507 kPa (73.5 psi). Generally, for the same pressurized spray system, the droplet size, breakup velocity and mass flow flux are all dependent on the nozzle pressure. To eliminate the coupling effects induced by these variables, all experiments were performed at a fixed nozzle pressure of 507 kPa. The pulsation of the diaphragm pump was significantly suppressed by the two in-line pressure regulators. During the experiments, the pressure fluctuations in the spray nozzle were controlled within ±1.7 kPa (0.25 psi). The spray flow rates at 507 kPa were calibrated to be 24.0 cm^3/min for WDB-0.5 and 89.2 cm^3/min for WDB-2.0. The impacting mass fluxes were changed by adjusting the distance from the nozzle to the heated surface. The spray mass fluxes were measured, using a catcher with a wet tissue placed horizontally to preserve the air flow pattern, to be between 0.19 and 1.50 g/cm^2 min for low spray mass flux tests and 4.41 g/cm^2 min for high spray mass flux tests. The droplet breakup velocity was estimated to be a fixed value of 31.9 m/s due to the constant pressure for both nozzles using a simple control volume energy balance around the nozzle [8].

2.2.2. Test bed

Fig. 3 shows the test bed used in the high-heat-flux tests. Test chips were mounted on the top side of the 1.0-mm thick aluminum support plate while the heater was attached to the bottom side. A thin (0.127 mm thick) layer of thermally conductive phase-change interface material (T-pcm 905C, Thermagon) was applied to both interfaces to minimize the contact resistances. The phase-change material has a thermal conductivity of 3.0 W/m K and, when heated to 50 °C, begins to flow to fill the interstitials between surfaces. Four 500-W cartridge heaters, controlled by a variac, were inserted to a 19-mm thick aluminum block as the heating source. Voltage and resistance of the heaters were measured using an HP34401A multimeter to obtain the power input. The resistance of the heaters had been calibrated at different temperature levels within the experiment range of operation. The heating block was then wrapped with a layer of ceramic insulating material to minimize heat loss. The only difference between low and high-heat-flux tests is the type of heater. A 250-W mica foil heater (Minco) with a diameter of 38.1 mm and a thickness of 0.51 mm was used for the low heat flux tests. The total heat loss of the system was measured using thermocouples located at different radial positions on the aluminum surface beyond the heated zone and evaluated for the surrounding insulation to be less than 12% and 7% of the power input in low and high-heat-flux tests, respectively.

2.3. Data acquisition system

Two sheathed 0.25-mm-diameter J-type (iron–constantant) thermocouples were buried between the test surface

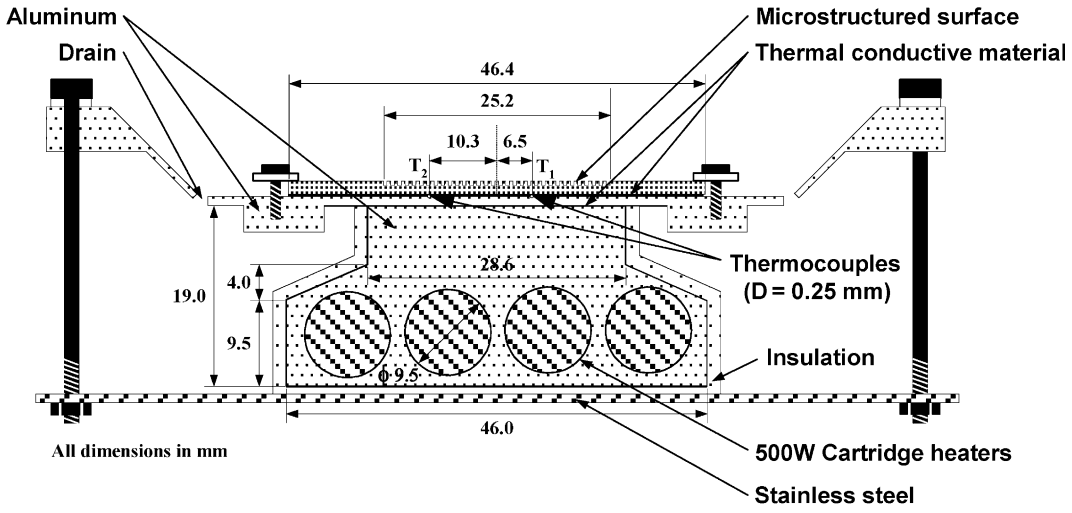

Fig. 3. Schematic of the miniaturized test bed for high-heat-flux tests.

and the support plate in Fig. 3. The two thermocouples were positioned at a distance of 6.5 and 10.3 mm from the test surface center to monitor the temperature uniformity. Temperature readings were sampled by a data acquisition system, and stored in a personal computer. The temperatures were extrapolated to the bottom surface of the grooves to evaluate the surface temperatures (T_1 and T_2) by assuming one-dimensional heat conduction along the direction perpendicular to the surface.

2.4. Experimental procedures

Before each run, the vacuum pump was applied for 30 min. The test surface was flushed sequentially by 0.1 M hydrofluoric acid and distilled water, followed by acetone, methanol and distilled water to wash off any organic residual remaining on the surface. After the spray mass flux was verified, the power was turned on and set to the desired voltage. The system was considered in steady state after surface temperatures remained constant for at least 5 min. The surface temperatures were then recorded for 2 min or longer. The electric power would shut off if the entire silicon surface was mostly dry or the heater was likely to undergo burnout.

2.5. Uncertainty analysis

The primary experimental variables are the surface heat flux, surface temperature, and spray mass flux. Individual measurement errors are either equal to the 95% confidence level of the calibration data or provided by manufacturers. The estimation of uncertainty for the derived experimental variables is based on the method of propagation of errors. The uncertainty in the surface heat flux measurement was found to be less than 4.1% and 3.7% for high and low heat flux tests, respectively. Considering the thermocouple calibration error and extrapolation error, the maximum uncertainty of the surface temperature was evaluated to be less than 0.7 K. The uncertainty in the spray mass flux was estimated to be smaller than 5.0% by taking into account of the pressure uncertainty and positioning errors.

3. Results and discussion

All the experiments in the present study were conducted in an open environment to facilitate the observation of the evolution process of water film on micro-textured silicon surfaces at elevated temperatures (heat fluxes). Heat transfer data presented in this study are based on the base surface area, i.e. $25.2 \times 25.2\ \text{mm}^2$. Heat transfer results of the plain silicon surface were used as reference to emphasize the performance improvement due to the surface micro-textures. The effect of dissolved gas in FC-72 has been reported by Horacek et al. in [15]; however, it was found that the dissolved nitrogen in water in the present tests has insignificant effects on heat transfer performance.

The focus of the present study is to investigate the heat transfer characteristics of evaporative spray cooling on micro-textured silicon surfaces. In addition, different surface materials were used to determine the effects of the surface's wettability. Heat transfer results of different spray mass fluxes and system orientations are also presented in the following sections.

3.1. Effects of surface material

Fig. 4 shows the heat transfer curves of water spray cooling on the plain silicon and aluminum surface at spray mass fluxes of 1.50 and 4.41 g/cm^2 min. Due to its more wettable surface property with water, the aluminum surface allows higher heat transfer rates in the test ranges. The spreading of a liquid film on a surface, which is strongly related to the liquid affinity (wettability) to the surface, has a significant effect on the evaporative heat transfer, as a more wettable surface results in a larger and thinner liquid film, which promotes evaporation.

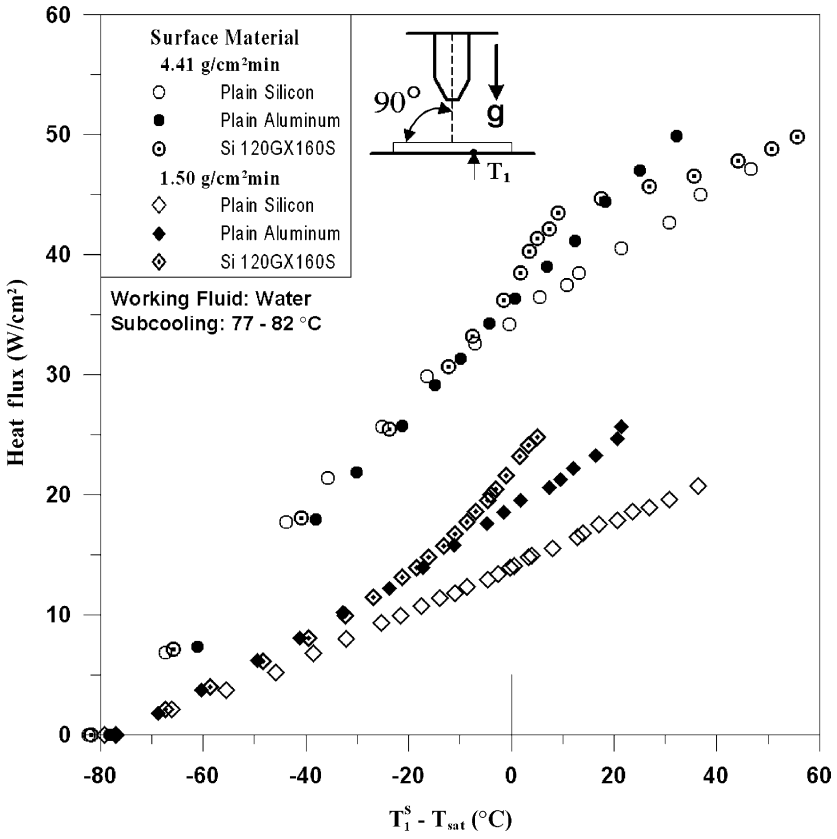

Fig. 4. Heat transfer performance for the plain silicon surface, plain aluminum surface and surface 120G × 160S at spray mass flux of 1.50 and 4.41 g/cm^2 min.

Furthermore, if the sprayed liquid has lower affinity for the heating surface, the deposited liquid film will be easier to be displaced out of the heat transfer area by the impinging droplets, resulting in a poorer coolant usage.

A contrary trend on the effect of surface's wettability on evaporative spray cooling was reported by Sehmbey et al. [16]. They asserted that a less wettable surface provides a higher possibility for nucleation and, hence delivers a better cooling performance. However, unlike most metals, which have a very large number of nucleation cavities on the surface, the silicon surface used here is single-crystal and almost free from surface defects, which means that the silicon surface has much fewer nucleation sites for boiling to occur. In fact, the surface roughness in their study is about 20 times higher than that measured on the polished silicon surface. Furthermore, since the spray mass fluxes used in their study are much higher than those in this study, the heat transfer surfaces were always flooded. As can be clearly seen in Fig. 4, no boiling was observed on the plain silicon surface in all tests.

It is also of great interest to note that regardless of lower heat transfer rate for a plain silicon surface, surface 120G × 160S does possess a higher heat transfer capability than a plain aluminum surface in the thin film regime. This suggests that the drawbacks of using less wettable surface for evaporative cooling be overcome by the adoption of surface enhancement.

3.2. Effects of surface texture

The primary objective of surface enhancement on plain silicon surfaces is to take advantage of capillary force to passively spread the impinging liquid droplets, and to ensure the formation of a thinner liquid film for efficient evaporation. A qualitative study of evaporation of a single water droplet on plain and textured silicon surface is given, followed by a quantitative study of evaporative spray cooling on different textured silicon surfaces.

3.2.1. Evaporation of a single droplet

The evaporation history of a water droplet sitting on a plain and textured silicon surface is depicted in Fig. 5. As illustrated in Fig. 5(a), the evaporation of the water film on the plain silicon surface, initially having a contact angle of θ, continues over a constant wetted area until the receding contact angle (θ_r) is reached. Then, the contact line (the boundary line common to all three phases) recedes and the contact angle of the liquid film recovers to a value between the advancing and receding contact angles. Note that this contact angle θ' may be different from the previous one (θ) due to the dissimilar microscopic surface conditions. The static advancing and receding contact angle of water on silicon are measured on inclined surface under microscope to be about 65° and 20°, respectively. This evaporation–contraction process repeats until the droplet is totally

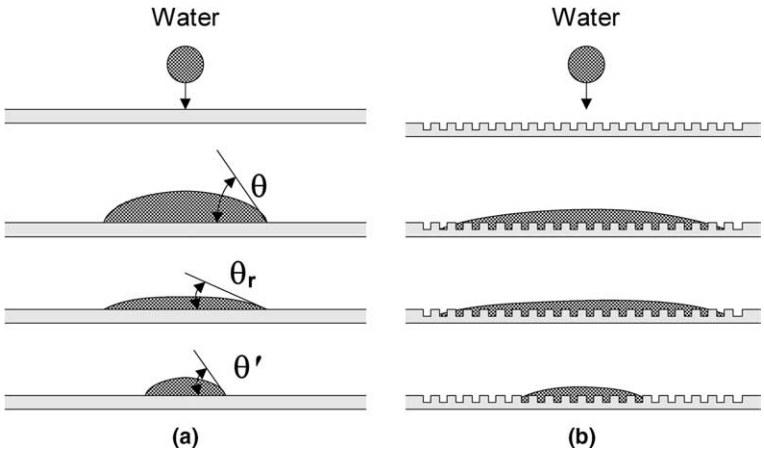

Fig. 5. Evaporation history of a single water droplet placed on (a) a plain silicon surface, (b) a micro-textured silicon surface.

evaporated. Since contact angle is a quantitative representation of a surface's wettability, it is obvious that, for a liquid droplet of a fixed amount, a more wettable (smaller contact angles) surface will have a larger average wetted area and therefore a thinner average film thickness during the entire evaporation process.

On the contrary, the liquid film on the micro-textured silicon surface in Fig. 5(b) holds the original contact line during most of time of evaporation, implying that the surface tension-induced contraction is balanced off by the capillary forces created between the micro-studs. Accordingly, the enhanced silicon surface gives a higher evaporative heat transfer rate than the plain silicon surface. Water droplets generated by a gauge-30 needle were gently placed on different test surfaces and their evaporation times were measured. The surface temperature of all test chips was kept at 80 °C to speed up the evaporation. The evaporation time is 64.6 s for the plain surface and 35.3 s for the surface $120G \times 160S$.

The liquid film evaporation on the surface $360G \times 480S$ was also examined. Unlike the surface $120G \times 160S$, the liquid film on the surface $360G \times 480S$ was torn into several smaller regions during the evaporation, indicating that the capillary forces existing between the micro-studs are not strong enough to keep the liquid film as a single entity. Consequently, the average available heat transfer area reduces and the average film thickness increases. The evaporation time for the surface $360G \times 480S$ is 43.5 s, which is longer than that on the surface $120G \times 360S$ but still shorter than that on a plain surface.

3.2.2. Heat transfer characteristics

The evaporative cooling of a water spray on micro-textured silicon surfaces can be generally divided into four distinct regions with different liquid film distribution patterns as shown in Fig. 6(a) and (b). The heat transfer characteristics of the evaporative spray cooling is significantly affected by the surface conditions. In region I, the flooded regime, the entire micro-textured surface is covered by a thick liquid film. At 4.41 g/cm^2 min, the thickness of the liquid film above the top surface of the test chips is about 75–100 μm at the center and 150–200 μm around the edge of the micro-textured area, as measured under microscope when compared with the size of studs. The heat transfer is mainly contributed by the forced convection induced by the direct droplet impingement plus, to a lesser extent, by evaporation from the free surface. The effect of surface enhancement is limited and the heat transfer rates for all surfaces are about the same (within experimental errors) as shown in Fig. 7.

As the surface heat flux increases, the liquid film on the micro-textured surfaces becomes thinner, and finally part of stud surfaces (usually the center area) are exposed to the impinging droplets. The liquid film thinning process continues until the surface is totally dry. At the same time, the area of dry stud surfaces expands towards the edges. This is identified as region II, the thin film regime. The upper bound of this regime is the film breakup point, which is defined as the situation at which at least one spot on the base silicon surface is in direct contact with the impinging droplets. The thin liquid film substantially enhances the evaporation from the free surface and equivalently, the overall heat transfer. This enhancement is indicated by the increase in the heat transfer coefficients of the micro-textured surfaces in Fig. 7. Fig. 7 also shows that the highest heat transfer coefficient of the textured surface occurs just right before the liquid film breakup. It is worth to note that no boiling was observed within the liquid film, except some spots around the edge of the textured area where the liquid film is thicker.

The thin liquid film will finally break up beyond a certain temperature, and dry patches will appear. The surface is now in region III, the partial dryout regime. Since the heat dissipation through dry patches is much less effective than that through the liquid film, the excess heat must be removed by the neighboring liquid film. This aggravates the consumption of liquid film. Consequently, the heat transfer in this regime declines severely as seen in Fig. 7.

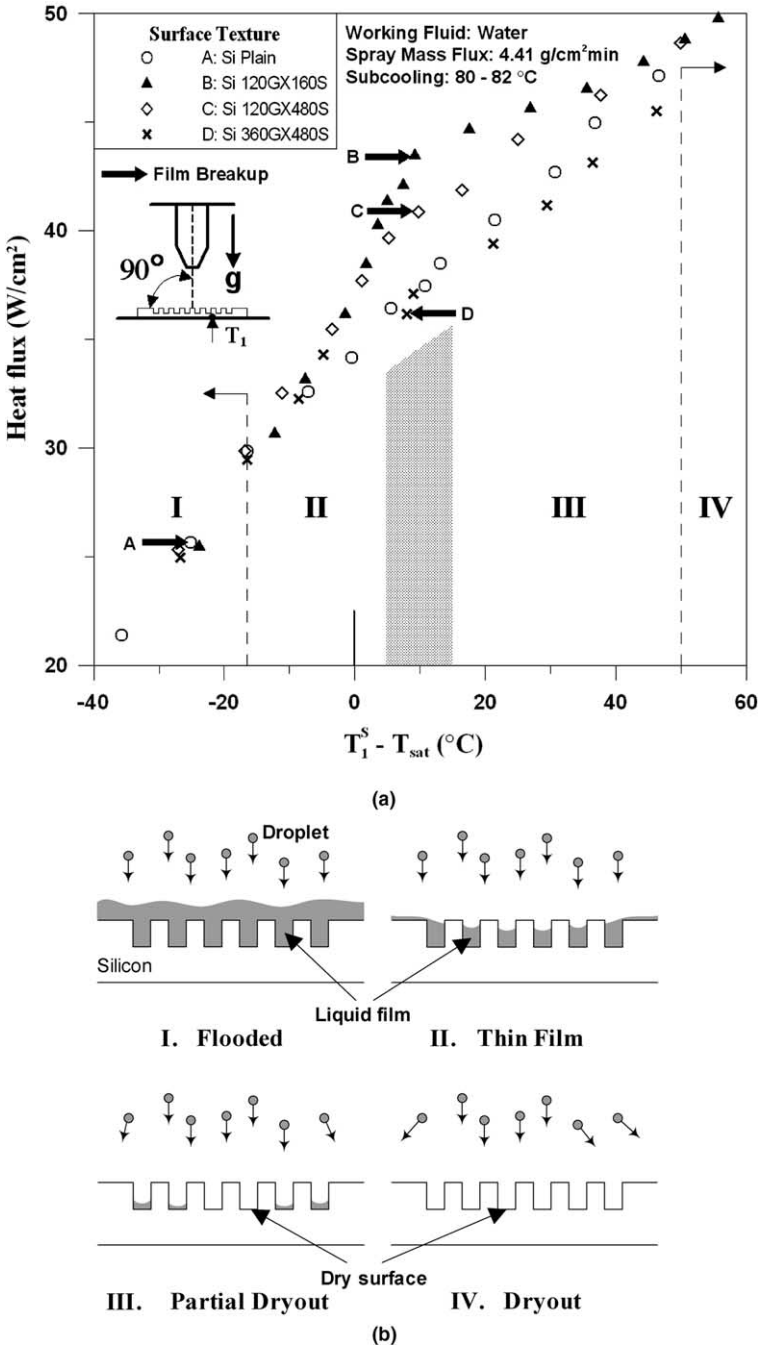

Fig. 6. (a) Heat transfer results of four different surface textures (upward-facing surface) at spray mass flux of 4.41 g/cm^2 min. (b) Schematic of the four heat transfer regimes on the micro-textured surfaces.

The liquid film pattern on the textured surface in region III is very sensitive to the local variations in experimental conditions. For example, the perturbation in droplet impingement or surface heat flux may recover the dry patches at some spots but create other dry patches at the same time. Due to the repeating cycles of the liquid film breakup and recovery, the surface temperature in this regime is neither spatially uniform nor temporally consistent. The partial dryout regime is similar to the transition-boiling regime in nucleate pool boiling.

As surface temperature increases further, eventually, no liquid film exists on the surface and the entire surface is dry. This is region IV, the dryout regime. In this regime, the heat removal mainly relies on the evaporation of the impinging droplets. The liquid droplets evaporate and form a vapor barrier against the access to the surface of the coming droplets when the vapor escapes from the hot surface. Compared to the inertia force of the impinging droplets, the force of the resulting vapor flow is so strong that the droplets can be drifted away from their course

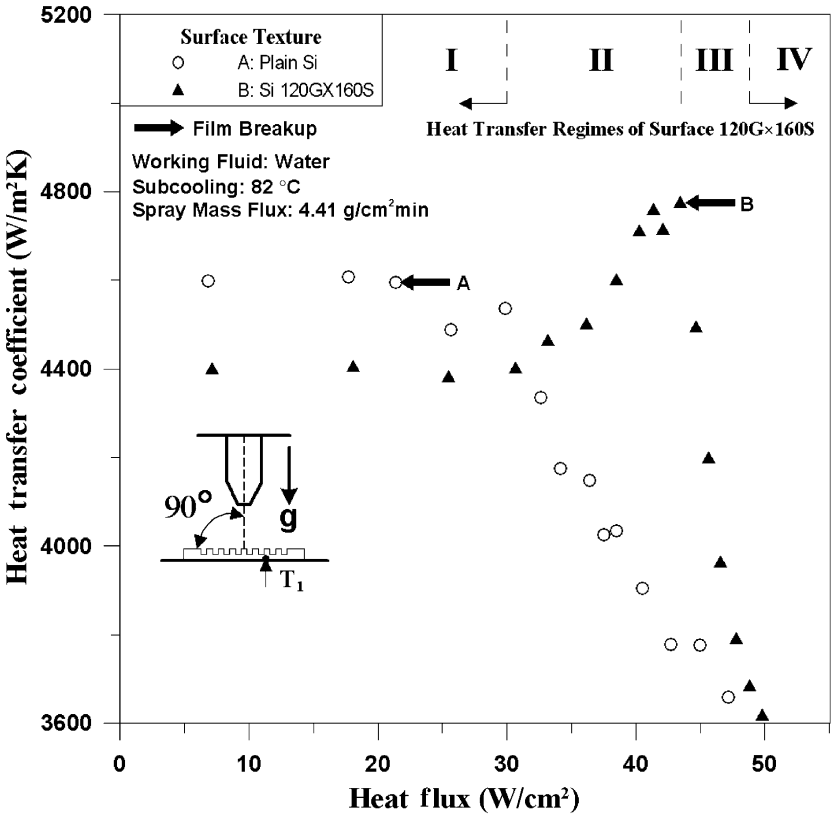

Fig. 7. Heat transfer coefficients for the plain silicon and 120G × 160S surface at spray mass flux of 4.41 g/cm^2 min.

toward the heated surface. The heat transfer rate is hence determined by the amount of liquid droplets arriving at the surface. As shown in Figs. 6(a) and 7, the heat transfer curves for all surfaces converge in this region, indicating that the surface enhancement, as a result, has negligible effect on the heat transfer characteristics.

3.2.3. Spray cooling on different micro-textured surfaces

As shown in Fig. 6(a), all the micro-textured surfaces are able to maintain the full liquid film coverage over the heated surface to higher heat fluxes, and have higher heat transfer rates in the thin film regime. The capillary force between the microstructures provides an effective means to counteract the shear drag exerted by the spray. More coolant is saved on the heated surface. On the other hand, due to the early liquid film breakup, the coolant utilization efficiency of a plain silicon surface in the thin film regime is much lower. As grooves are narrower, the capillary force becomes more effective in spreading and holding the liquid over the heat transfer surface, resulting in a wider liquid coverage and thinner liquid film for better evaporative heat transfer. This comparative wicking effect can be related to the Bond number defined in Eq. (1). Effective heat transfer area is another important variable under investigation. Although the total heat transfer area of the textured surfaces was augmented by at least 124%, the resulting heat transfer enhancement is much less than that in all regimes. In the flooded and dryout regime, the effect of surface pattern is insignificant. In the thin film and partial dryout regimes, the heat is primarily dissipated by evaporation through the free surface of the liquid film. The most relevant heat transfer area is hence the bottom surface of the grooves. The top and sidewall surface of the studs are of relatively less importance.

As seen in Fig. 6(a), the heat fluxes of the surface 120G × 160S and 120G × 480S are 17% and 10%, respectively, higher than the plain silicon surface at about the same surface temperature right before the film breakup point. The two surfaces have the same *Bo*. The difference in the heat flux enhancement between these two surfaces is the consequence of the difference in the surface area of the groove bottom. However, the heat transfer enhancement deteriorates greatly as the groove width increases from 120 to 360 μm, while keeping the surface area of the groove bottom constant. The heat transfer rate of the surface 3600G × 480S is only slightly higher than that of the plain surface in the thin film regime, and becomes worse once the liquid film breakup appears. The above discussion implies that, within the experimental range, the Bond number of the groove is the primary surface parameter responsible for the heat transfer enhancement of evaporative spray cooling on micro-textured silicon surface.

The surface temperature fluctuations are random in nature. The ranges of fluctuation are plotted against the heat flux in Fig. 8. Due to the thermal inertia, the real range of fluctuation could be larger than measured here. Only

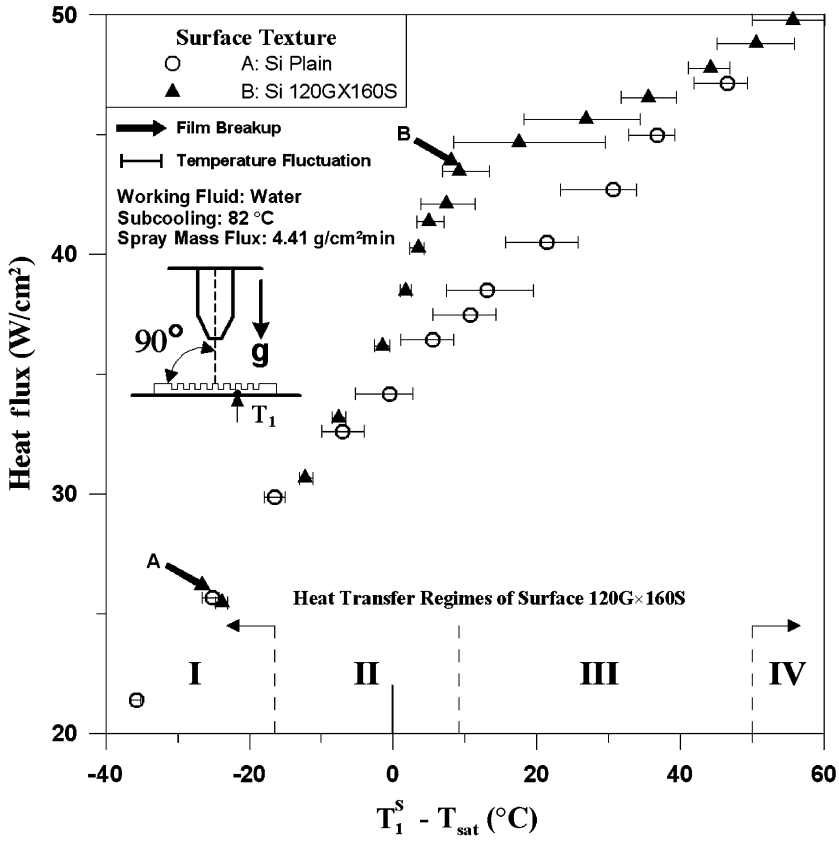

Fig. 8. Surface temperature fluctuations of the plain silicon and 120G × 160S surface at spray mass flux of 4.41 g/cm^2 min.

the results of the plain and 120G × 160S surface are presented, as the surface 120G × 480S and 360G × 480S have similar behavior as the surface 120G × 160S. The surface temperature of the plain and enhanced surfaces maintains stability as long as the liquid film breakup has not occurred.

3.2.4. Liquid film breakup heat flux

As discussed previously, the performance of low-mass-flux evaporative spray cooling on enhanced silicon surfaces, including heat transfer rate, surface temperature uniformity and temperature stability, deteriorates greatly once the liquid film breakup occurs. The susceptibility to high surface temperature and temperature fluctuations and non-uniformity of the high-heat-flux electronics restricts the system from operating beyond the liquid film breakup point.

Fig. 9 shows the liquid film breakup heat fluxes at different Bond numbers. It can be clearly seen that Bond number is the primary factor in determining the liquid film breakup heat flux within the test range. A general trend is that the smaller the Bond number, the higher the liquid film breakup heat flux. Ideally, there could be an optimal Bond number because when Bond number goes to zero the surface is essentially a smooth flat one. In this experiment, the range of the Bond number is not wide enough to demonstrate this. An important factor not considered here is the solid surface property such as the wettability of the surface (or the contact angle). Since the wettability of the surface is a direct index of the liquid film spreading ability, it is reasonable to speculate that the liquid film breakup point is also a function of the surface material. Therefore, the extension of the current results to liquids and surfaces other than water and silicon is appropriate if the effects of the contact angle on the liquid film breakup can be clearly identified

3.3. Effect of spray mass flux

Fig. 10 shows the effect of spray mass flux. Higher heat transfer rates are observed at higher spray mass fluxes. For a nozzle at the same inlet pressure, a higher spray mass flux means a higher droplet impact frequency on the heat transfer surface. In other words, more liquid is available for heat dissipation at the same period of time. However, as indicated in Fig. 10, the effect of spray mass flux in the flooded regime is not as pronounced as that in the thin film regimes and beyond. This is because the heat transfer in the flooded regime is not limited by the coolant supply rate.

3.4. Effects of system orientation

System orientation effects on evaporative spray cooling were investigated by rotating the whole system with respect to the gravity. The effects of system orientation are of great importance while applying the concept of evaporative

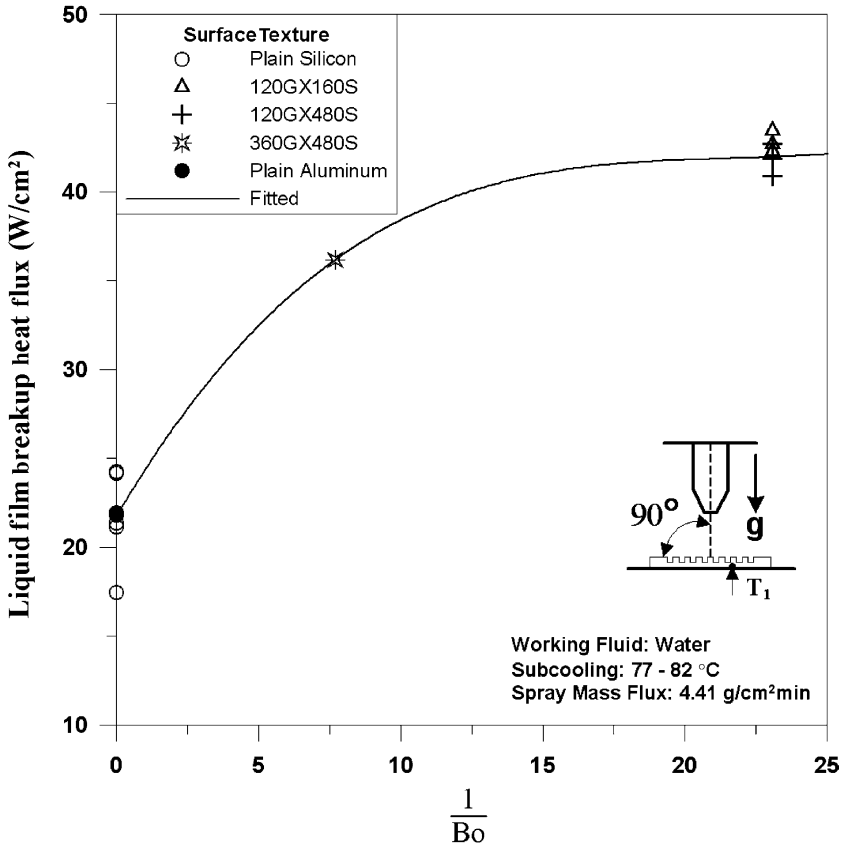

Fig. 9. Liquid film breakup heat fluxes for surfaces with different Bond numbers.

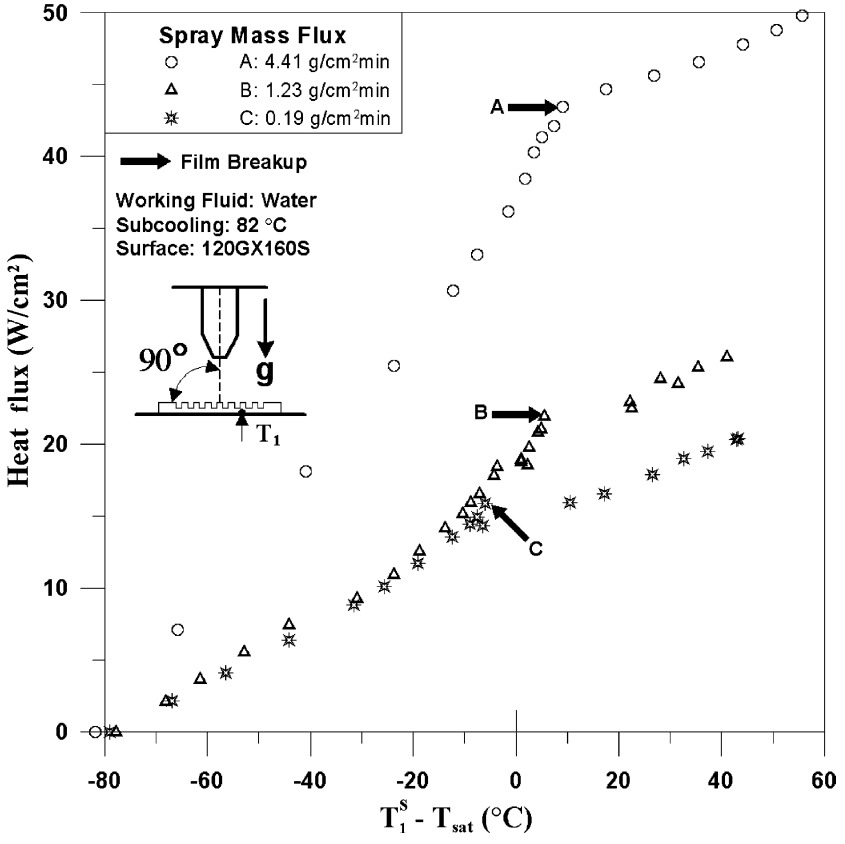

Fig. 10. Heat transfer performance for different spray mass fluxes of the surface 120G × 160S.

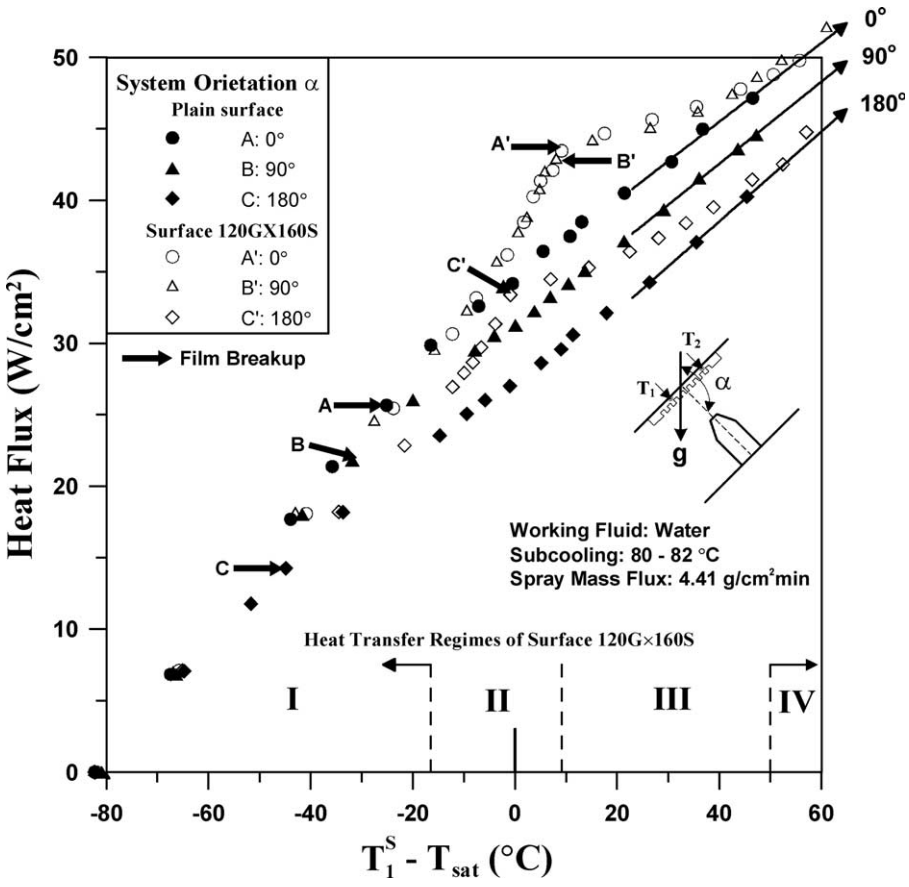

Fig. 11. Heat transfer performance for different system orientations of the plain silicon and 120G × 160S surface at spray mass flux of 4.41 g/cm^2 min.

spray cooling in portable electronic devices. The system orientation affects both the ability of the liquid film attachment to the heated surface when thin film evaporation is dominant, and the accessibility of the impinging droplets to the heated surface when the counter-flowing vapor flow is significant. Fig. 11 shows the heat transfer results of the plain and textured surface at three different system orientations, i.e. $\alpha = 0°$, 90° and 180°. For all the system orientations, the surface 120G × 160S provides higher cooling capability and higher liquid film breakup heat fluxes than the plain surface. However, the results for both surfaces converge to a single line after the surface dries up, as the surface enhancement has negligible effect on heat transfer characteristics in the dryout regime. In addition, the film breakup heat fluxes of both surfaces decrease as the system orientation changes from upward-facing ($\alpha = 0°$) to vertical ($\alpha = 90°$), and downward-facing ($\alpha = 180°$), implying the detrimental liquid film detachment effect caused by the gravitational force. The downward-facing surface has the worst cooling performance among the three orientations. When a droplet approaches the surface, the counter-flowing vapor escaping from the heated surface pushes against the droplet inertia. For a downward-facing surface, as opposed to an upward-facing surface, gravity is also against the droplet inertia. Consequently, fewer droplets are able to reach the heated surface, resulting in a lower heat transfer.

Fig. 11 also shows that the performance of $\alpha = 90°$ is comparable to that of $\alpha = 0°$. This improvement can be attributed to the reduced counteracting force induced by the vapor flow, and the overflow from the upper part of the test chip. It should be noted that the spray coverage is larger than the textured area.

4. Conclusions

Experiments were carried out to investigate the evaporative heat transfer characteristics of spray cooling of water on micro-textured silicon surfaces at very low mass fluxes. The qualitative study of evaporation of a single water droplet sitting on the plain and micro-textured silicon surfaces suggests that the microstructures provide an effective means to enhance the evaporation rates. Four distinct heat transfer regimes, which are the flooded regime, the thin film regime, the partial dryout regime and the dryout regime, were observed. Surface texture has negligible effect on heat transfer performance in the flooded and dryout regimes, because the heat transfer surface is totally covered by liquid in the flooded regime and by vapor in the dryout regime. However, in the thin film and partial dryout regime, the

micro-textured surfaces give higher heat transfer rates than the plain silicon surface. The capillary force within the microstructures is effective in spreading the deposited liquid film over the heated surface and keeping the surface wetted to a higher heat flux. Heat transfer coefficient and temperature stability deteriorate greatly once dry patches appear on the surface. The liquid film breakup heat flux increases as the Bond number of the microstructures decreases.

Surfaces with various Bond numbers and surface areas of the groove bottom were tested. It was found that the Bond number of the microstructures is the primary factor responsible for the heat transfer enhancement of evaporative spray cooling on micro-textured silicon surface in the present study. The effect of surface material was also examined in this study. A plain aluminum surface performs better than a plain silicon surface due to the more wettable surface property. However, the drawbacks of using a silicon surface as the heat transfer surface can be overcome by the adoption of surface enhancement. The micro-textures surface $120G \times 160S$ also provides higher heat transfer rates than the plain silicon surface in all systems orientations. The systems with downward-facing orientation have the lowest heat transfer rate in this study, because the gravity works against the droplet inertia such that less liquid is supplied to the heated surface. Increasing spray mass flux has a positive effect on the evaporative heat transfer rates, but the effect is not obvious in the flooded regime.

References

[1] K.A. Park, A.E. Bergles, Boiling heat transfer characteristics of simulated microelectronic chips with detachable heat sinks, in: Proceedings of 8th International Heat Transfer Conference, 1986, p. 4.

[2] H. Honda, H. Takamatsu, J.J. Wei, Boiling of FC-72 on silicon chips with micro-pin-fins and submicron-scale roughness, J. Heat Transfer 124 (2002) 383–390.

[3] R.W. Knight, D.J. Hall, J.S. Goodling, R.C. Jaeger, Heat sink optimization with application to microchannels, IEEE Trans. Components, Hybrids, Manufact. Technol. 15 (1992) 832–842.

[4] M.B. Bower, I. Mudawar, High flux boiling in low flow rate, low pressure drop mini-channel and micro-channel heat sinks, Int. J. Heat Mass Transfer 37 (1994) 321–332.

[5] D.C. Wadsworth, I. Mudawar, Enhancement of single-phase heat transfer and critical heat flux from an ultra-high-flux simulated microelectronic heat source to a rectangular impinging jet of dielectric liquid, J. Heat Transfer 114 (1992) 764–768.

[6] K.A. Estes, I. Mudawar, Comparison two-phase electronic cooling using free jets and sprays, J. Electron. Packaging 117 (1995) 323–332.

[7] S.C. Yao, S. Deb, N. Hammouda, Impacting spray boiling for thermal control of electronic systems, in: Proceedings of National Heat Transfer Conference, 1989, HTD-111.

[8] M. Ghodbane, J.P. Holman, Experimental study of spray cooling with Freon-113, Int. J. Heat Mass Transfer 34 (4) (1991) 1163–1174.

[9] M.S. Sehmbey, L.C. Chow, O.J. Hahn, M.R. Pais, Effect of spray characteristics on spray cooling with liquid nitrogen, J. Thermophys. Heat Transfer 9 (4) (1995) 757–765.

[10] S. Toda, A study of mist cooling (2nd report: Theory of mist cooling and its fundamental experiments), Heat Transfer—Jpn. Res. 3 (1) (1974) 1–44.

[11] M.R. Pais, L.C. Chow, E.T. Mahefkey, Surface roughness and its effects on heat transfer mechanism in spray cooling, J. Heat Transfer 114 (1992) 211–219.

[12] J.H. Kim, S.M. You, S.U.S. Choi, Evaporative spray cooling of plain and microporous coated surface, Int. J. Heat Mass Transfer 47 (2004) 3307–3315.

[13] C. Bonacina, S.D. Giudice, G. Comini, Dropwise evaporation, J. Heat Transfer 101 (1979) 441–446.

[14] D.P. Rini, R.-H. Chen, L.C. Chow, Bubble behavior and nucleate boiling heat transfer in saturated FC-72 spray cooling, J. Heat Transfer 124 (2002) 63–72.

[15] B. Horacek, K.T. Kiger, J. Kim, Single nozzle spray cooling heat transfer mechanisms, Int. J. Heat Mass Transfer 48 (2005) 1325–1438.

[16] M.S. Sehmbey, M.R. Pais, L.C. Chow, Effect surface material properties and surface characteristics in evaporative spray cooling, J. Thermophys. Heat Transfer 6 (3) (1992) 505–512.